Effect of mass flow rate on gas propagation after vacuum break in a liquid helium cooled tube.

IOP Conf. Series: Materials Science and Engineering **755** (2020) 012112 doi:10.1088/1757-899X/755/1/012112

Effect of mass flow rate on gas propagation after vacuum break in a liquid helium cooled tube.

Nathaniel Garceau[1,2], Shiran Bao[1], Wei Guo[1,2]

[1]National High Manetic Field Laboratory, Tallahassee, FL 32310 USA
[2]Mechanical engineering department, FAMU-FSU College of Engineering, Tallahassee, FL 32310 USA

Email: wguo@magnet.fsu.edu

Abstract. Vacuum break in particle accelerators is a major concern due to risks associated with personnel and extensive equipment damage. Continuing research in our lab focuses on the sudden loss of vacuum in the liquid helium cooled beam-line tubes of superconducting particle accelerators. In our previous research, we studied nitrogen gas propagation in a uniform tube system immersed in both normal helium (He I) and superfluid helium (He II). It was observed that He II has a stronger effect in slowing down the gas propagation compared to He I, but this effect was largely due to the variation of the point where condensation and deposition of the nitrogen gas on the tube inner wall. Here, we discuss our modifications to the tube system that now allow us to accurately control the starting location of gas condensation in both the He I and He II experiments. Systematic studies of gas propagation were conducted using this new tube system by varying the nitrogen mass flow rate at the tube inlet.

1. Introduction

Vacuum failure in cryogenic systems, such as particle accelerators or cryogenic liquid storage tanks, is a major concern due to personal dangers and costly equipment damage. Loss of vacuum in these systems causes a huge heat load to be exerted on the cryogenic liquids, which boils the liquids rapidly. Rapid boiling of the cryogens can cause a dangerous buildup in pressure and possibly lead to injuries or system damage [1].

Superconducting linear particle accelerators are long cryogenic systems composed of interconnected segments called cryomodules. Cryomodule are designed with two vacuum spaces [2]. First is an internal evacuated niobium cavity bathed in liquid helium (LHe) where the particles travel and second the bath insulating vacuum layer with multi-layer insulation. Vacuum break into the insulating layer is often, but not always, confined to a cryomodule. Vacuum break into the particle beam tube is more a concern because all the niobium cavities of the system are interconnected. If a vacuum break occurs in the beam tube, the whole system could be affected by air and dust as the gas propagates in the system. To mitigate some of the risks of damage and contamination, fast acting valves linked to the beam-line's vacuum are generally used to prevent the inrushing gas from spreading to multiple cryomodules. To evaluate the risks and help mitigate possible damages in a loss of vacuum scenario, multiple failure studies at accelerator labs have been conducted [3-5].

Vacuum failure into a particle accelerator's beam tube has two linked aspects to how far and fast the gas propagates: shock tube vacuum break and cryopumping. Shock tube problem is a well studied and modeled problem [5-6]. A shock wave of gas forms and propagates in the tube following the vacuum break. Second aspect is linked to the process known as cryopumping. Cryopumping is the process during which gas molecules collide with and condense or freeze to a cold surface. This process is known and has been the topic of prior research [7]. To understand vacuum failure in particle accelerators both shock tube over a long distance and cryopumping must be studied together. Previous studies incorporating vacuum break and cryopumping have been reported but the studied systems' dimensions were limited so gas propagation was not a major factor [8-10]. To expand the understanding of what happens in an beam tube several experiments were conducted and showed that the propagating gas front slows down substantially when traveling in a freezing vacuum channel such as an accelerator's beam tube. Fermi National Accelerator Laboratory and at European X-ray free-electron laser (XFEL) conducted several experiments which showed propagating gas velocities on the order of 10 m/s, which are orders of magnitude lower than the shock tube experiments velocities [5,11,12].

To achieve a better understanding of this slowing down process, first experiments in our lab conducted by Dhuley and Van Sciver verified this slowing down effect and then they clarified that the observed slowing was due to gas condensation to the wall [13-15]. Preliminary experiments which they conducted also indicated that there was a much stronger slowing effect in He II cooled tubes compared with He I [15]. Expanding upon their work in an upgraded helical tube system, we verified that there was indeed a difference between He I and He II. However, our analysis indicated that the uninsulated cold section of the tube above the liquid level plays a significant role in the differences seen in the data between the two helium phases [16]. The point at which condensation begins occurs in the section of tube above the liquid level is different between the two phases due to different filling methods and requirements for operation of the experiments. In the He I experiments, the helium was slowly filled up to the desired location, which causes the condensation point to be closer to the liquid level. Whereas in He II experiment, the tube above the liquid level is significantly cooled due the LHe bath being filled to a higher location and then it undergoes an evaporative cooling step to reach the He II phase. This difference in filling methods changes the temperature profile above the liquid level and causes the condensation point to shift higher above the liquid level in the He II experiments.

For this paper, we elaborate on system modifications which took place to fix the condensation point to a known location. Also, we expand upon the initial experiments and start looking at the effect of mass flow rate on the gas propagation. The systematic variation of mass flow rates variations were also conducted to look at the effect of mass flow rate. This paper also summarizes our previously published preliminary model which systematically described the momentum, mass and heat transfer processes occurring after the dynamic event of a vacuum break.

2. Experiment

2.1. System Changes

Our lab's first experiments by Dhuley and Van Sciver used a straight tube immersed in LHe for both simplicity and ease of fabrication [13-15]. Due to issues with low level of LHe during the He II experiments, the system was changed to a copper helical tube design to allow a long section of tube to remain immersed after evaporative vacuum pumping [16]. The helical tube is 5.75 m in length, has a 2.8 cm outer diameter copper tube, has a wall thickness of 1.25 mm. The tube was coiled in a 22.9 cm diameter with a pitch of 5.1 cm. The helical system uses a 230 L nitrogen buffer tank to provide gas during the extent of the run.

The helical tube system encountered an issue with exaggerated slowing down effect in He II experiments due a shifting condensation point caused by evaporating cooling above the liquid helium bath. To fix the condensation point to a known location, a 7.6 cm stainless steel vacuum shield was added with multi-layer insulation around the 2.8 cm stainless extension pipe which connects the outer plumbing to the inner LHe immersed helical tube. To set the temperature profile within the vacuum

jacket, a Kapton tape heater was wrapped around the base of the inner tube just before the exit of the vacuum jacket. A Lake Shore 340 Temperature Controller and a Lake Shore Cernox® sensor was used to control and monitor the temperature in this lower section of the tube. The location of the control sensor is approximately 35 mm above the copper elbow stainless steel transition external to the vacuum jacket. For the experiments, the controller temperature was set to 77 K, which is the condensation point of nitrogen at 1 atm. Three additional E-type thermocouples were spot-welded to the inner extension tube's surface at 65 mm, 265 mm and 465 mm above the copper elbow stainless steel transition such that the tube temperature profile would be known. Figure 1 (a) shows the basic system schematic. Figure 1 (b) shows the CAD drawing illustrating more details of the vacuum jacket assembly.

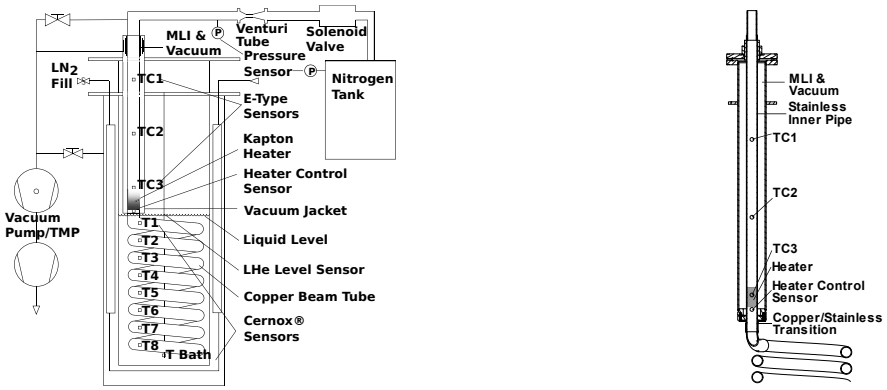

(a) (b)

Figure 1. (a) Basic schematic of upgraded helical beam tube system and (b) a CAD drawing of new vacuum jacket assembly.

To control the mass flow rate, the 230 L buffer tank was charged with 50, 100, 150 and 200 kPa absolute of pure nitrogen gas (99.999% pure). To simulate the break in vacuum a fast-acting solenoid valve (25 ms opening time) was positioned after the buffer tank. Immediately after the solenoid valve, a venturi pipe was used to choke the gas flow into the evacuate beam tube by limiting the gas velocity to the speed of sound at the venturi pipe's throat. To calculate mass flow, gas pressure was monitored in the buffer tank with a 344 kPa (50 psia), 0-10 V pressure transducer. Mass flow calculations using this transducer data were conducted following Dhuley's method detailed in [13-15].

To measure the gas propagation in the helical copper tube, seven or eight Lake Shore Cernox™ thermometers were encapsulated in 2850 FT Stycast® epoxy and mounted to the tube's surface following Dhuley's method [17]. To mount the sensors the copper tube was slightly deformed and then polished to create a level area which the senor could sit. The eight sensors were placed at 72 cm intervals and secured with a stainless steel hose clap or twisted wire. Between the tube the encapsulated sensor indium foil and Apiezon® N thermal grease was used to minimize contact resistance.

To monitor and record pressure and temperature data at high speeds, the sensors were wired into four Data Translation, Inc. DT9824 USB data acquisition modules and recorded with National Instruments LabView™ at a frequency of 4800 Hz.

The liquid helium level in the system was monitored with a superconducting liquid helium level sensor positioned in the centre of the helical tube spiral. With the sensor allowed consistent filling to the same location between experiments, which was the stainless steel-copper transition at the exit of the vacuum jacket.

Liquid helium in the experiment boils rapidly due to the very large heat load induced by the incoming gas. To prevent pressure build-up in the system two large diameter 3 psi safety valves were on the vent exit. A third slightly smaller 5 psi safety valve was also added to the top mounting flange of the system.

2.2. *Data processing*

After opening the solenoid valve, arrival of the gas front location was marked by a sudden spike in temperature on the tube wall and is referred to as the 'rise time,' *t*. In order to extract the rise time, the temperature data was smoothed using an 80-point moving average to remove random and harmonic noise within the data. This method was similar to what has been used in prior experiments [13-16]. Threshold level for He I was set at 100 mK over the bath temperature, which is 4.2 K for LHe at 1 atm. This level was above the sensor noise and in the nearly vertical region of the temperature data. For the He II experiments, the threshold was set at 25 mK above the bath temperature which, was monitored by the sensor in the center of the helical coil. This was done because the bath temperature gradually rises over the course of the experiment and a lower value was available due to less noise. Figure 3 shows smoothed temperature over time data for 100 kPa He I and He II experiment runs with the threshold marked by horizontal lines and vertical lines indicating the rise time. From Figure 2 (b) one can see the temperature rises due to the incoming heat load then it flattens as the temperature approaches the lambda transition point. This profile is expected due to the large specific heat of LHe in the transition region and indicates that the LHe remained in the He II phase while the data was recording.

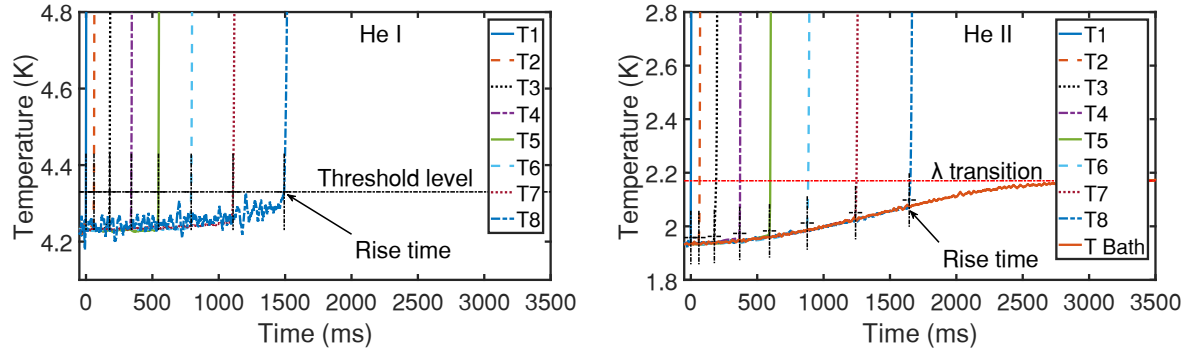

Figure 2. Smoothed experimental data for He I (a) and He II (b) with a buffer tank pressure of 100 kPa. Threshold level is indicated by a dashed horizontal line(s). Rises time for each sensor is indicated by the short vertical lines. (color online)

3. Results

3.1. Insulation effect

In previous experiments, we showed that there was likely a shift in condensation point of the nitrogen entering the system during the He I and He II experiments [16]. For the new insulated system with the temperature controller set at 77 K, temperatures of the upper section of the tube were 250 K, 210 K and 150 K, which was well above the critical point of nitrogen. For the non-insulated experiments for the He II the upper temperature profile was 60 K, 15 K and 3 K [16]. This temperature profile change affected the rise times of the various sensors. For example, for the non-insulated system setup rise times for sensor T8 were 1400 ms for He I and 2000 ms for He II yet for the insulated system, rise times were about 1500 ms for He I and 1600 ms for He II. Timing difference shows that there still is a stronger slowing effect in He II but not as strong as seen previously.

Following Dhuley's method in [13-15], to characterize the slowing effect rise time data for each wall sensor for both LHe phases were fitted using a non-linear squares regression method in the form:

$$t(x) = a\left(e^{x/b} - 1\right) \quad (1)$$

Where *a* and *b* are the fit parameters and represent the decay time and propagation decay length. *t(x)* is the arrival time at location *x* and $x = 0$ is considered the condensation point of the gas. For the non-insulated case, the exact condensation point wasn't known and was assumed to be at the liquid, but previous analysis showed this likely was not true [16]. For upgraded system with insulation, the condensation point was fixed in the 35 mm region between the heater and at the exit of the vacuum

jacket which was at the LHe bath temperature. The exit of the vacuum jacket is fixed to be the $x = 0$ location.

Figure 3 shows a comparison between the He I and He II experiments for the insulated and non-insulated cases. From the figure, the He I and He II data curves are much closer together for the insulated case compared with the non-insulated case. This difference is the result of fixing the condensation point by adding the insulation. Whereas the non-insulated case, the unknown condensation point could vary significantly between runs.

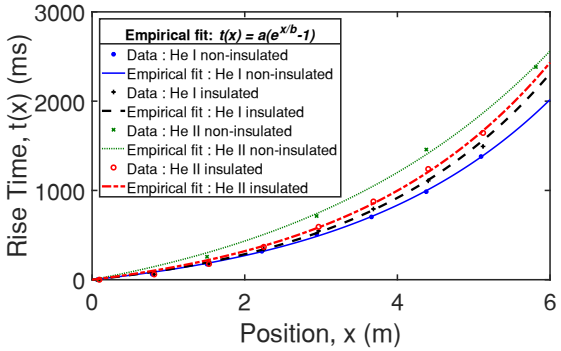

Figure 3: He I and He II experiment rise times as a function of position for both insulated and non-insulated cases.

The arrival time-location curve above was converted into a velocity equation in the following form:

$$v = v_o \cdot e^{-x/b} \quad (2)$$

where $v_o=b/a$ is the entrance velocity at $x = 0$, the assumed or known condensation point [13-15]. Previous research observed that the calculated entrance velocities were different due a different condensation point above the liquid level [16]. Table 1 lists the fitted coefficient values a and b as well as the calculated v_o for 100 kPa buffer tank pressure for both insulated and non-insulated experiments.

From Table 1, the calculated entrance velocities are much closer together. For the non-insulated case, He I and He II experimental entrance velocities difference is over 4 m/s. Whereas the velocity is around 1 m/s for the insulated case. This new data shows much better consistency between the two different LHe phases and allowed for the next steps to be taken to look at the effect of mass flow on the data.

Table 1: Fitted coefficients of the decay time, a, and the decay length, b, with the calculated entrance velocity, v_o.

	a(s)	b(m)	$v_o=b/a$ (m/s)
Non-insulated He I	0.247	2.71	10.95
Non-insulated He II	0.561	3.50	6.23
Insulated He I	0.237	2.53	10.66
Insulated He II	0.286	2.67	9.30

3.2. Mass flow effect

To understand how mass flow into the insulated beam tube affected gas propagation, the mass flow was varied by changing the buffer tank pressure. Buffer tank pressure was set at 50 kPa, 100 kPa, 150 kPa and 200 kPa. Average calculated mass flow based on pressure drop of the buffer tank following Dhuley's method for each fill pressure was 9.8 g/s, 18.3 g/s, 26.1 g/s and 35.2 g/s respectively [13].
From figure 4, the arrival times increase as mass flow rate decreases for both He I and He II. When the mass flow rate is low enough freeze out will occur. Freeze out is when mass flow rates are small and all the gas sticks to the surface of the tube before reaching the full length of the pipe. The seventh sensor in the 50 kPa cases did not rise due to freeze out. Given adequate time, the sensor would have eventually risen but this was outside the time scope of these experiments due to limited gas supply in buffer tank.

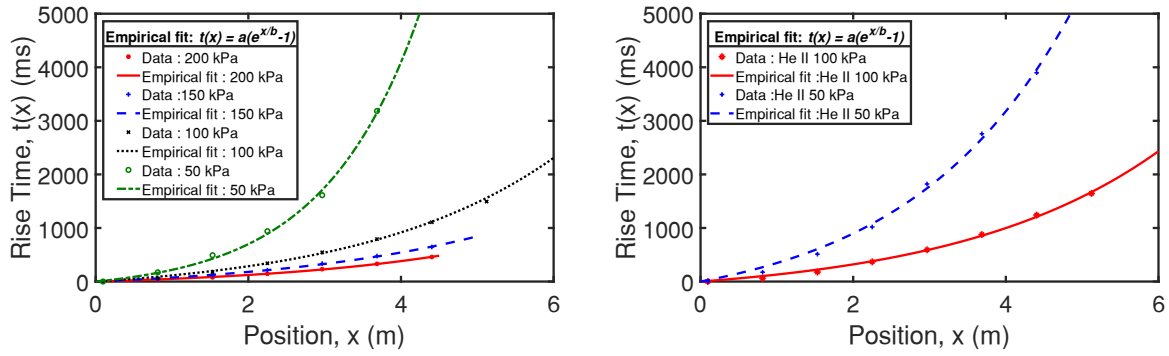

Figure 4. Effect of mass flow rate on arrival times for He I (a) and He II (b) experiments.

4. Theoretical modelling

4.1. Preliminary model

We have previously explored issues with Dhuley and Van Sciver's conservation mass flow based model and developed a new systematic model [16]. To summarize our preliminary developed 1-D model, we used three main gas dynamics equations to more quantitatively describe the deceleration of the gas. First equation was for the conservation of energy:

$$\frac{\partial}{\partial t}\left[\rho\left(\varepsilon+\frac{1}{2}v^2\right)\right]+\frac{\partial}{\partial x}\left[\rho v\left(\varepsilon+\frac{1}{2}v^2+\frac{P}{\rho}\right)\right]=-\frac{4}{D_1}m_c\left(\varepsilon+\frac{1}{2}v^2+\frac{P}{\rho}\right)-\frac{4}{{D_1}^2}Nu\cdot k\left(T_g-T_s\right) \quad (3)$$

Second equation was for the conservation of mass:

$$\frac{\partial\rho}{\partial t}+\frac{\partial}{\partial x}(\rho v)=-\frac{4}{D_1}\dot{m}_c \quad (4)$$

The final gas dynamics equation was for the conservation of momentum:

$$\frac{\partial}{\partial t}(\rho v)+\frac{\partial}{\partial x}(\rho v^2)=-\frac{\partial P}{\partial x}-\frac{4}{D_1}\dot{m}_c v \quad (5)$$

Symbol nomenclature for (3) – (5) and subsequent equations is provided in Table 2.

Table 2. Theoretical model nomenclature

Variable	Description	Variable	Description
ρ	Gas bulk density	R	Ideal gas constant
ρ_w	Gas density at the wall surface	Nu	Nusselt number
v	Gas velocity	$\dot{m}_c$	Condensation mass flow rate
P	Gas equilibrium pressure	$\dot{m}_o$	Mass flow rate toward tube wall
P_s	Gas saturated vapour pressure at surface temperature	x	Position along the tube
T_g	Gas temperature	D_1	Tube inner diameter
M	Gas molar mass	D_2	Tube outer diameter
$\hat{h}_g$	Gas enthalpy	T_s	Tube wall surface temperature
$\hat{h}_s$	Solid nitrogen enthalpy	k	Tube wall thermal conductivity
ε	Internal energy of the ideal gas	q	Heat flux into the wall
C	Effective sticking coefficient	q_{he}	Heat flux into the liquid helium
S_w	Specific heat of the wall material		

The additional terms in (3) – (5) on the right hand side of the equations are related to the mass deposition process at the inner tube wall surface. Using kinetic theory of gasses, mass deposition is expressed by multiplying an effective sticking coefficient, C, by the total mass flow rate toward the wall:

$$\dot{m}_c = \dot{m}_o \cdot C\left(T_g, T_s, P\right) = \rho \sqrt{\frac{RT_g}{2\pi M_g}} \cdot C\left(T_g, T_s, P\right) \tag{6}$$

Sticking coefficient is a function of the temperature of both the gas and the wall surface. In the free molecular flow region, research shows that the sticking coefficient is dominantly controlled by the wall temperature when the gas temperature is relatively low [7-10]. In the continuum flow region the dynamics in the variation of C are more complex and is still a study of active research. For this preliminary simulation, the sticking coefficient of nitrogen was set to 0.6 at low temperatures and approaches zero as it increases toward the condensation temperature [16].

Radial heat transfer and tube wall temperature was modelled by solving the radial heat transfer equation:

$$\rho_w S_w \frac{D_2^2 - D_1^2}{4D_1} \frac{\partial T_s}{\partial t} = q - q_{he} \frac{D_2}{D_1} \tag{7}$$

Equation (7) was adopted from Dhuley and Van Sciver [13-15] and neglects the effect of the building nitrogen frost layer on the tube surface. Heat flux into the saturated helium bath, q_{he}, was evaluated based on published empirical heat transfer models for film boiling, nucleate boiling and convective heat transfer [17,18]. Heat flux into the wall, q, is due to both gas convection and gas condensation and is modelled by:

$$q = \dot{m}_c \left[\frac{1}{2}v^2 + \hat{h}\left(T_g, P\right) - \hat{h}\left(T_s, P_s\right)\right] - \frac{Nu \cdot k}{D_1}\left(T_g - T_s\right) \tag{8}$$

For our experiments and for this model nitrogen gas is always close to unity therefore its state is described by the ideal gas equation of state:

$$PM = \rho R T_g \tag{9}$$

(3)-(9) were solved simultaneously using Godunov's two-step scheme in Python to determine how gas propagates within the system [22].

This preliminary model underwent verification by comparing it to the 100 kPa experimental data and has been previously published in [16]. Figure 5 (a) shows a summary of our previous simulation results and figure 5 (b) shows the corresponding experimental He I wall temperature profiles in the insulated system. The two temperature profiles on similar locations on the pipe show qualitatively similar behaviour. The model captured the sensor temperature spike as the gas arrives and it also captured how the temperatures saturate at a specific temperature as the front passes. Behaviour of both graphs are the result of decreasing gas density and velocity down the tube. The form of the numerical model captured the main physics of the gas propagation along a LHe cooled tube but it was noted that the rise times and exact temperatures differ from the measured values. This was due to the simplification of the preliminary model by excluding conduction resistance from the nitrogen frost layer and simplification of the sticking coefficient model. In an upcoming paper, we will elaborate on an expanded and refined model which quantitatively compares our experimental measured data to the simulation data.

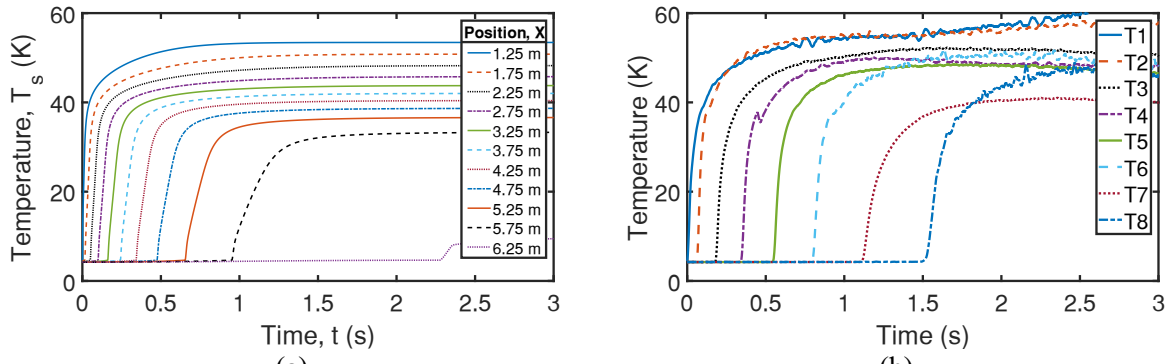

(a) (b)

Figure 5. Comparison of the behaviour of simulated wall temperatures (a) with actual experimental data (b).

5. Conclusion

This paper describes the continuing research into expanding and modelling the sudden loss of vacuum in beam-line liquid helium cooled particle accelerators. Our system has been improved by adding an insulating jacket to the upper portion of the tube. Data showed that calculated entrance velocities of the two helium phase experiments were much closer together and the jacket was effective in mitigating variation in the condensation point. Systematic studies varying mass flow rate were also conducted to also observe the effect of changing mass flow rate. Our published numerical model that systematically describe gas dynamics of the setup was briefly summarized with experimental data.

For future, the numerical model will be expanded and refined to include other factors which were neglected in the initial simulation such as the effect of the frost layer. Furthermore, mass flow rate variation experiments conducted in this experiment will need to be simulated using the expanded model to further validate the refined model. Additional experiments at different mass flow rates to better assess the overall model are also planned. Final planned variation of the experimental system is to change the tube diameter and compare it to the refined model.

6. References

[1] Flynn T 2005 *Cryogenic Engineering: 2nd Revised and Expanded*, CRC Press, Florida
[2] Padamsee H 2018 Cornel University, CLASSEE, New York (Accessed July 2019) <https://arxiv.org/ftp/arxiv/papers/1501/1501.07129.pdf>
[3] Wiseman M, Crawford K, Drury M, Jordan K, Preble J, Saulter Q and Schneider W 1994 *Adv. Cryogenic Engineering* **39** 997-1003
[4] Seidel M, Trines D and Zapfe K 2006 Failure analysis of the beam vacuum in the superconducting cavities of the TESLA main linear acclerator, TESLA-Report 2002-06
[5] Ady M, Vandoni G, Guinchard M, Grosclaude P, Kersevan R, Levallois R and Faye M 2014 (Technical report) Retrieved from CERN Database, (EDMS No. 1414574)
[6] Takiya T, Higashino F, Terada Y and Koumura A 1999 *J. Vac. Sci. and Tech.* **A 17(4)** 2059-63
[7] Dawson J and Haygood J 1965 *Cryogenics* **5(2)** 57-67
[8] Brown R, Trayer D and Busby M 1970 *J. Vacuum Science and Technology* **7-1** 241-6
[9] Rogers K 1996 (Techical contractor report) Retrieved from National Aeronautics and Space Administration, Technical Reports Server (Report No. NASA-CR-553)
[10] Bosque E 2014 (Dissertation), Retrieved from Florida State University, Proquest Publishing database (UMI No.3625730)
[11] Heidt C and Grohmann S 2014 *Adv. Cryo. Eng.: Trans. Cryo. Eng. Conf.* AIP Pub. 1574-80
[12] Boeckmann T, Hoppe D, Jensch K, Lange R, Maschmann W, Peterson B and Schnautz T 2009 *Proc. Of the Int. Cryogenic Eng. Conf. 22 – Cryogenic Materials Conf.-2008, Seoul* 723-8
[13] Dhuley R and Van Sciver S 2016 *Int. J. Heat and Mass Transfer* **96** 573-81
[14] Dhuley R and Van Sciver S 2016 *Int. J. Heat and Mass Transfer* **98** 728-37
[15] Dhuley R 2016 (Dissertation) Retrieved from Florda State University, Proquest Dissertations Publishing database (UMI No.10120583)
[16] Garceau N, Bao S and Guo W 2019 *Int. J. of Heat and Mass Transfer* **129** 1144-50
[17] Dhuley R and Van Sciver S 2016 *Cryogenics* **77** 49-52
[18] Bland M 1975 *Cryogenics* **15** 639-43
[19] Davey G 1976 *Vacuum* **26** 17-22
[20] Van Sciver S 2012 *Helium Cryogenics 2nd* Springer Science+Business Media LLC, New York
[21] Steward W 1978 *Int. J. Heat Mass Transfer* **21(7)** 863-74
[22] Sod G 1978 *J. Computational Physics* **27** 1-31

Acknowledgments

This work is supported by U.S. Department of Energy grant DE-FG02-96ER40952. The experiments were conducted at the National High Magnetic Field Laboratory, which is supported by NSF DMR-1157490 and the State of Florida.